

## **Experimental demonstration of a magnetically induced warping transition in a topological insulator mediated by rare-earth surface dopants**

Beatriz Muñiz Cano, Yago Ferreiros, Pierre A. Pantaleón, Ji Dai, Massimo Tallarida, Adriana I. Figueroa, Vera Marinova, Kevin García Díez, Aitor Mugarza, Sergio O. Valenzuela, Rodolfo Miranda, Julio Camarero, Francisco Guinea, Jose Angel Silva-Guillén, Miguel A. Valbuena

This version of the article has not been peer-reviewed and is presented “as is”. In the case the article has been later published to a peer-reviewed journal, a link to the version-of-record of the article is provided as an alternative URI in the metadata record.

### **To cite this version**

Beatriz Muñiz Cano, Yago Ferreiros, Pierre A. Pantaleón, Ji Dai, Massimo Tallarida, Adriana I. Figueroa, Vera Marinova, Kevin García Díez, Aitor Mugarza, Sergio O. Valenzuela, Rodolfo Miranda, Julio Camarero, Francisco Guinea, Jose Angel Silva-Guillén, Miguel A. Valbuena. Experimental demonstration of a magnetically induced warping transition in a topological insulator mediated by rare-earth surface dopants. 3<sup>rd</sup> February 2023.

<https://repositorio.imdeananociencia.org/handle/20.500.12614/3275>

### **Licensing**

Use of this version is subject to the author terms of use, specified in the metadata record.

# Experimental demonstration of a magnetically induced warping transition in a topological insulator mediated by rare-earth surface dopants

Beatriz Muñiz Cano,<sup>†</sup> Yago Ferreiros,<sup>†</sup> Pierre A. Pantaleón,<sup>†</sup> Ji Dai,<sup>‡</sup> Massimo Tallarida,<sup>‡</sup> Adriana I. Figueroa,<sup>¶,§</sup> Vera Marinova,<sup>||</sup> Kevin García Díez,<sup>‡,§</sup> Aitor Mugarza,<sup>§,⊥</sup> Sergio O. Valenzuela,<sup>§,⊥</sup> Rodolfo Miranda,<sup>†,#</sup> Julio Camarero,<sup>†,#</sup> Francisco Guinea,<sup>†,@</sup> Jose Angel Silva-Guillén,<sup>†</sup> and Miguel A. Valbuena<sup>\*,†</sup>

<sup>†</sup>*Instituto Madrileño de Estudios Avanzados, IMDEA Nanociencia, Calle Faraday 9, 28049, Madrid, Spain*

<sup>‡</sup>*ALBA Synchrotron Light Source, 08290, Cerdanyola del Vallès, Barcelona, Spain*

<sup>¶</sup>*Departament de Física de la Matèria Condensada, Universitat de Barcelona, 08028 Barcelona, Spain.*

<sup>§</sup>*Catalan Institute of Nanoscience and Nanotechnology (ICN2), CSIC and BIST, Campus UAB, 08193, Barcelona, Spain*

<sup>||</sup>*Institute of Optical Materials and Technologies, Bulgarian Academy of Sciences, Acad. G. Bontchev, Str. 109, 1113, Sofia, Bulgaria*

<sup>⊥</sup>*ICREA Institució Catalana de Recerca i Estudis Avançats, Lluís Companys 23, 08010, Barcelona, Spain*

<sup>#</sup>*Departamento de Física de la Materia Condensada; Instituto “Nicolás Cabrera” and Condensed Matter Physics Center (IFIMAC), Universidad Autónoma de Madrid (UAM), Campus de Cantoblanco, 28049, Madrid, Spain*

<sup>@</sup>*Donostia International Physics Center, Paseo Manuel de Lardizábal 4, 20018, San Sebastián, Spain; and Ikerbasque, Basque Foundation for Science, 48009, Bilbao, Spain*

E-mail: miguelangel.valbuena@imdea.org

## Abstract

Magnetic topological insulators constitute a novel class of materials whose topological surface states (TSS) coexist with long-range ferromagnetic order, eventually breaking time-reversal symmetry. The subsequent bandgap opening is predicted to co-occur with a distortion of the TSS warped shape from hexagonal to trigonal. We demonstrate such a transition by means of angle-resolved photoemission spectroscopy on the magnetically rare-earth (Er and Dy) surface-doped topological insulator  $\text{Bi}_2\text{Se}_2\text{Te}$ . Signatures of the gap opening are also observed. Moreover, increasing the dopants coverage results in a tunable p-type doping of the TSS, thereby allowing for gradual tuning of the Fermi level towards the magnetically induced bandgap. A theoretical model where a magnetic Zeeman out-of-plane term is introduced in the hamiltonian governing the TSS rationalizes these experimental results. Our findings offer new strategies to control magnetic interactions with TSSs and open up viable routes for the realization of the quantum anomalous Hall effect.

Topological insulators (TI) define a state of matter where the strong spin-orbit interaction (SOI) induces an exotic metallic topological surface state (TSS) with relativistic, Dirac-like, band dispersion with the spin locked to the momentum in an otherwise insulating material<sup>1,2</sup>. Magnetic impurities interaction with the TSSs is especially attractive in these materials due to the emergence of novel quantum phenomena with relevant fundamental and technological implications in spintronics and quantum information processing<sup>3</sup>. The combination of topological properties and magnetic order can lead to new quantum states of matter as the quantum anomalous Hall effect (QAHE), characterized by purely spin-polarized dissipationless currents without an external magnetic field<sup>4,5</sup>.

When magnetism is introduced by impurity doping with magnetic elements, either via substitutional or surface doping<sup>6-9</sup>, magnetic extension<sup>10</sup>, or proximity coupling to magnetic layers<sup>11,12</sup>, the TI becomes magnetic (MTI) and the time-reversal symmetry (TRS) can be broken, magnetically inducing the opening of a bandgap at the Dirac point (DP) of the TSS<sup>6,7</sup>. If this gap is tuned to the Fermi level ( $E_F$ ), the QAHE can be realized as it was

first experimentally observed in Cr- and V- doped  $(\text{Bi,Sb})_2\text{Te}_3$  thin films<sup>13,14</sup>. Recent discoveries based on the magnetic extension of TIs, as the first antiferromagnetic TI (AFM),  $\text{MnBi}_2\text{Te}_4$ <sup>15,16</sup>, have opened up new perspectives for the realization of these quantized topological effects in intrinsically magnetic stoichiometric compounds. However, these systems heavily depend on sophisticated and complex growth methods, resulting in variations in the density of structural defects, eventually leading to drastic changes in the electronic structure of the TSSs (opening or not of an intrinsic magnetic gap at the DP) or affect its magnetic properties (formation or not of antiferromagnetic order)<sup>17</sup>. Similar discrepancies have been found because of inhomogeneities of the spatial distribution of bulk magnetic dopants<sup>18,19</sup>.

Surface doping offers an alternative to separate the two aforementioned critical processes, namely growth and doping, limiting the dopants presence to where the TSSs are most sensitive to their effects and maximizing the magnetic anisotropy by the lower coordination symmetry<sup>20</sup>. Experimental attempts at magnetically doped TIs surfaces also indicate that achieving control on the magnetic ground state and anisotropy is challenging due to the existence of multiple adsorption sites, strong surface relaxations, and significant doping of the bulk states from defects or inhomogeneities<sup>21–24</sup>. Although gaplike features have been interpreted as magnetically induced, numerous factors such as momentum and energy spatial fluctuations near the DP<sup>25</sup> or surface chemical modifications<sup>26–28</sup>, may contribute to the observation of a gap. Furthermore, the DP can be buried into the bulk band projections, making the possible gap opening undetectable by techniques as angle resolved photoemission spectroscopy (ARPES). These ambiguities evidence the necessity to go beyond the present state-of-the-art in the development of these doping strategies.

An alternative route to this problem is to surface-dope TIs with magnetic rare-earths (RE) whose larger size can prevent the occurrence of substitutional sites at the surface, reducing the multiplicity of adsorption configurations<sup>29</sup> and enhancing the magnetic anisotropy. Likewise, REs large magnetic moments, originating from the unpaired 4f electrons<sup>30</sup>, can maximize the magnetically induced gap hosting the spin-polarized currents<sup>7</sup>; and also allow

a lower doping concentration<sup>31</sup>, which could eventually lead to a robust QAHE at higher temperatures<sup>3</sup>. Besides, REs deposited on metals can be efficiently coupled via itinerant s and p electrons of the metal to achieve ferromagnetism with Curie temperatures as high as 80 K<sup>32,33</sup>. RE bulk substitutional doping with Eu<sup>34,35</sup>, Gd<sup>36</sup>, Dy<sup>31</sup> or Ho<sup>37,38</sup> on Bi<sub>2</sub>Te<sub>3</sub> thin films has been achieved. Eventhough the TSSs preservation despite REs large magnetic moments, all films remained essentially paramagnetic or weak AFM. Regarding the bandgap opening, massive Dirac fermions have only been observed for a given concentration of Dy-doped Bi<sub>2</sub>Te<sub>3</sub> thin films<sup>37</sup>. Magnetic proximity effects have also been explored on EuS layers on TI thin films with neither significant induced magnetism nor an enhancement of Eu magnetic moment at the interface<sup>39</sup>.

Recently, the magnetic order in MTIs, particularly in the newly discovered MnBi<sub>2</sub>Te<sub>4</sub> family<sup>40</sup>, have been theoretically predicted not to only open a gap at the DP, but to also lower the Dirac cone's warping symmetry from hexagonal to trigonal, alongside an induction of a gap opening at the DP<sup>41-44</sup>. Notably, this trigonal warping at the magnetically ordered phase is sensitive to the direction of a net surface magnetic moment, providing an effective approach for the detection of magnetic ordering effects on the TSSs when the gap cannot be unequivocally resolved and/or related to the TRS breaking by out-of-plane magnetic moments. However, an experimental observation of these phenomena is still lacking.

Herein, by means of ARPES, we report the effects on the TSS of the prototypical three-dimensional (3D) TI, Bi<sub>2</sub>Se<sub>2</sub>Te, doped with RE impurities (Er and Dy). As expected, the pristine surface features hexagonal warped TSSs which, as the RE atoms are deposited even for small coverages, exhibit the predicted transition from hexagonal to trigonal, providing the first experimental evidence of such magnetically induced warping modification. In addition, with the systematic doping, signatures of a bandgap opening at the DP are found, whereas the chemical potential is gradually modified resulting in a controllable p-type doping. This allows to tune the DP energy closer to the  $E_F$ , thus fulfilling the prerequisites for the realization of the QAHE. When the hamiltonian governing the TSS considers a net magnetic

moment, with an exchange field coupling of  $\approx 0.1$  eV, the experimental observations are rationalized.

Ternary  $\text{Bi}_2\text{Se}_2\text{Te}$  single crystals<sup>45</sup> were grown by a modified Bridgman method in a standard crystal growth system and characterized by X-ray powder diffraction and Raman spectroscopy (see Supplemental Material (SM)<sup>46</sup>), showing high crystal quality and crystalline long-range order. X-ray photoemission spectroscopy (XPS) and ARPES measurements were performed on *in situ* exfoliated single crystals (at  $T = 15$  K) with a MBS hemispherical analyzer at the LOREA beamline<sup>47,48</sup> in Alba Synchrotron, with linear horizontal polarization and photon energies of  $h\nu = 100$  eV and 52 eV, respectively. Er and Dy were sublimated with an e-beam evaporator. The deposition rates and coverages were calibrated with a quartz crystal microbalance and correlated with the attenuation of the XPS Bi 5d core level (SM<sup>46</sup>, Fig. S1). XPS and ARPES measurements were performed at  $T = 15$  K, well below the expected Curie temperature of Er and Dy clusters<sup>49</sup>, so a magnetic ordering of the RE surface dopants can be expected.

The  $\text{Bi}_2\text{Se}_2\text{Te}$  quintuple layer (QL) three dimensional (3D) crystal structure, and the Brillouin zone (BZ) and its projected surface Brillouin zone (SBZ) are sketched in Figs. 1(a)-(b), respectively.  $\text{Bi}_2\text{Se}_2\text{Te}$  bulk single crystals were mechanically exfoliated *in-situ* at 15 K to minimize the induced density of defects. The high sample quality is derived from the XPS spectrum (Fig. 1(c)), showing highly intense and narrow peaks with no signs of oxidation, contamination or large disorder<sup>28</sup> for the Se 3d, Te 4d and Bi 5d core levels. The very well defined spin-orbit doublets as compared to isostructural TI films grown by molecular beam epitaxy prove the surface quality after *in situ* exfoliation<sup>50-52</sup>.

Pristine  $\text{Bi}_2\text{Se}_2\text{Te}$  TSS ARPES bandmap along the  $\overline{\Gamma\text{M}}$  direction is shown in Fig. 1(d). At this photon energy ( $h\nu = 52$  eV) the bulk conduction band is above the  $E_F$ . The DP is located 415 meV below the  $E_F$ , outside the bulk projection bandgap, and the Fermi velocity is  $v_F \sim (6.0 \pm 0.3) \cdot 10^5$  m/s, estimated from  $1/\hbar (\partial E/\partial k)$ <sup>53</sup>, consistent with previous works<sup>53,54</sup>.

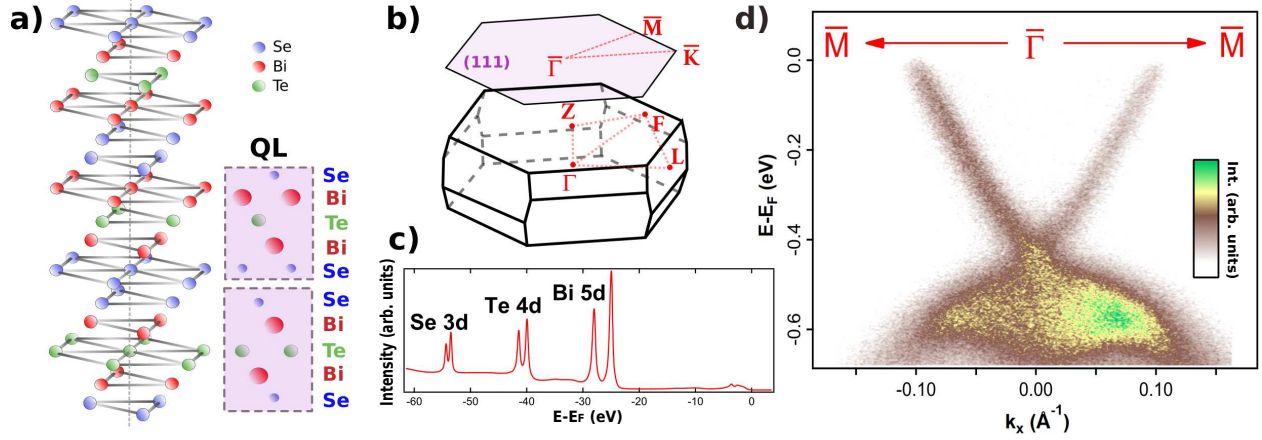


Figure 1: **Pristine  $\text{Bi}_2\text{Se}_2\text{Te}$  crystal structure and characterization.** (a) 3D quintuple layer crystal structure and (b) Brillouin zone (BZ) and projected surface BZ of  $\text{Bi}_2\text{Se}_2\text{Te}$ . (c) XPS spectrum (Se 3d, Te 4d, Bi 5d and valence band) of pristine  $\text{Bi}_2\text{Se}_2\text{Te}$  single crystal measured at a photon energy of  $h\nu = 100$  eV and at  $T = 15$  K. (d) ARPES bandmap of the pristine  $\text{Bi}_2\text{Se}_2\text{Te}$  TSS along the  $\overline{\Gamma\text{M}}$  direction acquired at  $h\nu = 52$  eV and at  $T = 15$  K.

Figure 2(a) displays XPS spectra showing the main effects on the core levels and the valence band (VB) states induced by Er deposition, as compared to the pristine sample. The Se 3d, Te 4d and Bi 5d core levels are attenuated (SM<sup>46</sup>, Fig. S3). No extra components are detected at higher binding energies (left side of the peaks), consistent with the absence of surface oxidation or contamination. Additionally, no further disorder is introduced since no widening of the peak line-shapes is detected; also evidenced by the very sharp, well resolved multippeak structure of highly localized and, in principle, weakly interacting (non-dispersive) Er 4f states at  $E-E_F = 5-12$  eV (magnified in the inset in Fig. 2(a)). The multippeak fit of the XPS spectra in Figs. 2(b)-(c) was used for the estimation of the Er-coverage. ARPES VB maps acquired at this energy region are included in the SM<sup>46</sup>, Fig. S2.

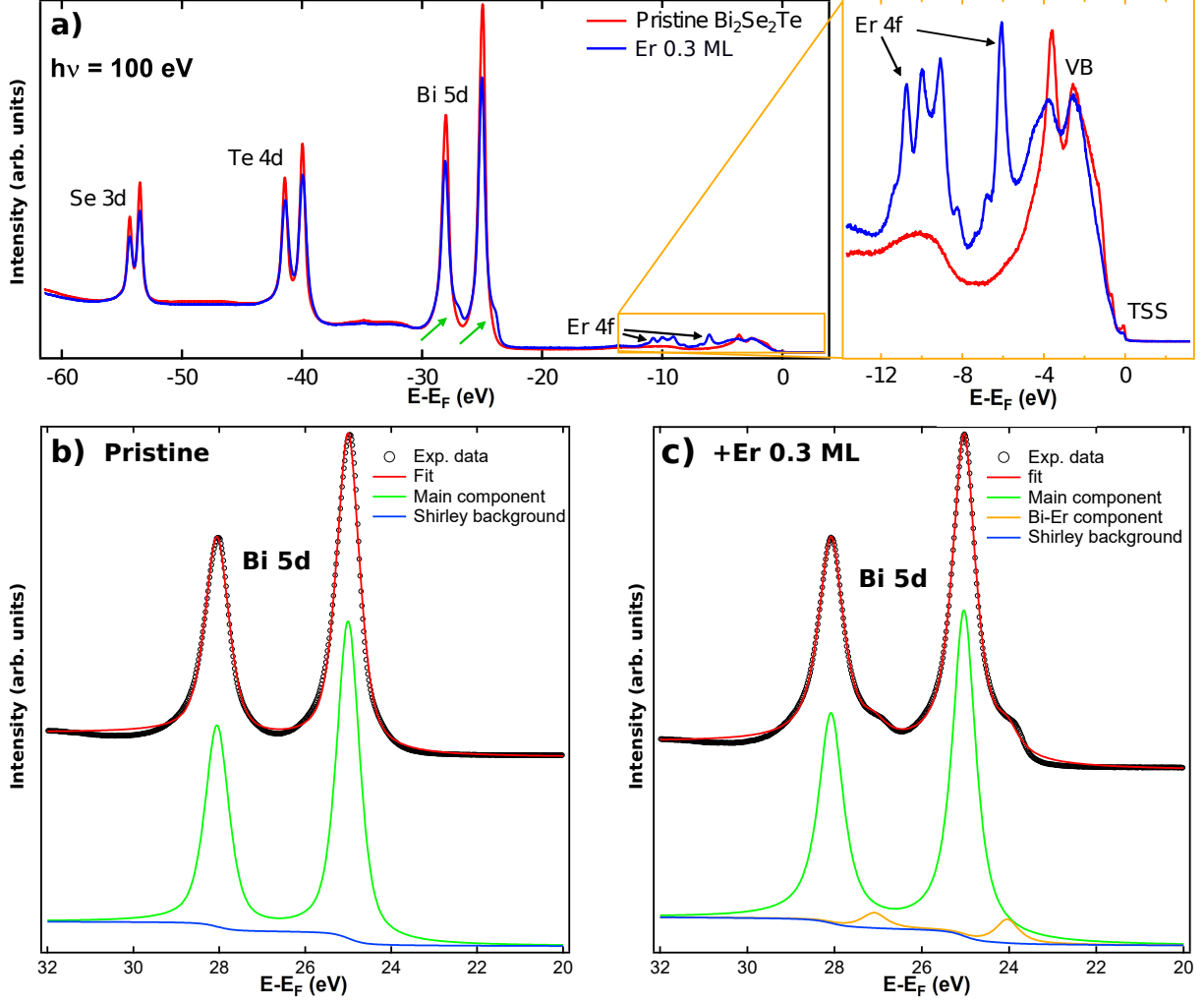


Figure 2: XPS characterization of Er-doped  $\text{Bi}_2\text{Se}_2\text{Te}$  acquired with a photon energy of  $h\nu = 100 \text{ eV}$  and at  $T = 15\text{K}$ . (a) Comparison of XPS spectra of pristine (red line) and 0.3 monolayer (ML) Er/ $\text{Bi}_2\text{Se}_2\text{Te}$  (blue line). A second component of the Bi 5d peak is developed after Er deposition (green arrows). Right: zoom-in on the Er 4f states and the  $\text{Bi}_2\text{Se}_2\text{Te}$  valence band energy range. Multipeak fit of XPS data for (b) the pristine sample and (c) the 0.3 ML Er-doped sample. A second component (orange) is related to Er-Bi interaction, as its area is proportional to the Er coverage (see SM<sup>46</sup>, Figs. S1 and S3).

Remarkably, a second Bi 5d component is developed at lower binding energies (green arrows in Fig. 2(a) and orange curve in Fig. 2(c)). These features intensity linearly increases with the Er coverage (SM<sup>46</sup>, Figs. S1 and S3), demonstrating its relationship with a superficial Bi-Er bond, and revealing a degree of interaction at the RE-TI interface. A charge transfer effect is also reflected in an energy shift as the Er content increases (see SM<sup>46</sup>, Fig. S1). A similar behavior has been observed for other metal-TI interfaces in the same Bi 5d

state<sup>51</sup>. Because of Bi and RE dopants larger atomic sizes, Bi-Er bonds are most likely to be formed than Se-Er or Te-Er ones, whose 3d and 4d states do not show extra components. The same Bi 5d second component also appears in Dy-doped Bi<sub>2</sub>Se<sub>2</sub>Te (SM<sup>46</sup>, Fig. S5).

The Fermi surface (FS) and constant energy (CE) maps for pristine and 0.3 monolayer (ML) Er/Bi<sub>2</sub>Se<sub>2</sub>Te are shown in Fig. 3. Pristine Bi<sub>2</sub>Se<sub>2</sub>Te TSS exhibits the hexagonal warped FS and the circular-like shaped lower energy CE maps expected for rhombohedral 3D TIs (Figs. 3(a)-(c)). The warping strength is consistent with the literature, being lower than in most warped TSSs, as in Bi<sub>2</sub>Te<sub>3</sub><sup>55,56</sup>, and higher than in isostructural Bi<sub>2</sub>Te<sub>2</sub>Se<sup>57</sup> or Bi<sub>2</sub>Se<sub>3</sub><sup>58</sup>, whose warping effects are smoother or even negligible. When depositing Er, the FS and CE maps drastically change. Upon 0.3 Er ML, the TSS warping symmetry evolves from hexagonal to trigonal (Figs. 3(d)-(f)), clearer away from the DP and closer to E<sub>F</sub>. Similar modifications in the Dirac cone warping, from hexagonal to trigonal, have been predicted below the magnetic ordering temperature in the family of MnBi<sub>2n</sub>Te<sub>3n+1</sub> MTIs<sup>42</sup>.

To give some insight into the warping transition of the TSS, the description of an undoped TI using the model developed by Fu<sup>55</sup> can be applied, in which the low energy dispersion of the system is described by the following Hamiltonian:

$$H = \hbar v_F (k_x \sigma_y - k_y \sigma_x) + \frac{\lambda}{2} (k_+^3 + k_-^3) \sigma_z, \quad (1)$$

with  $k_{\pm} = k_x \pm ik_y$ . The last term is only invariant under threefold rotation and responsible for the hexagonal warping<sup>41,42,55</sup>. The 3D band dispersion of the system is shown in Fig. 4(a), where the previously calculated  $v_F = 6.0 \cdot 10^5$  m/s was used to match the experiment. The warping parameter  $\lambda$  was set to  $175 \text{ eV} \cdot \text{\AA}^3$  by fitting the theoretical CE map at 0.415 eV (right-hand side of Fig. 4(a)) to the measured one (Fig. 3(a)). This value confirms a lower warping strength compared to other TIs such as Bi<sub>2</sub>Te<sub>3</sub><sup>55</sup>. The energy values (with respect to the DP) in the theoretical CE maps (Fig. 4(a)) were chosen to match the experiment (Figs. 3(a)-(c)). As expected, the hexagonal warping can be clearly distinguished far from

the DP whereas, when approaching the DP, the CE maps round off, as in the experiment (Figs. 3(a)-(c)).

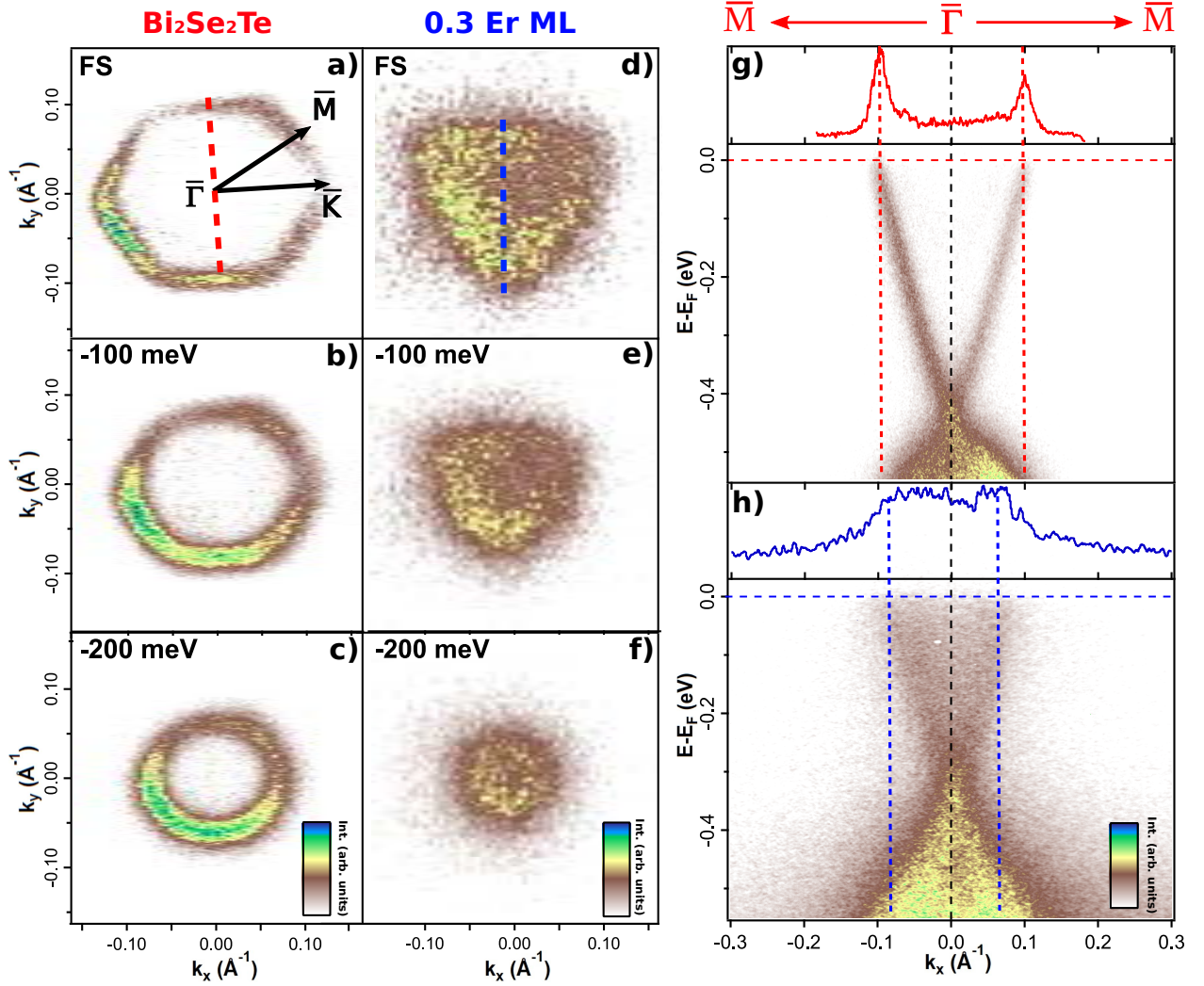


Figure 3: **Experimental observation by ARPES of the magnetically induced hexagonal to trigonal TSS warping transition upon Er deposition.** (a)-(c) Fermi surfaces and constant energy maps at 100 and 200 meV below the Fermi level ( $E_F$ ) for pristine  $\text{Bi}_2\text{Se}_2\text{Te}$ , showing the hexagonal warping of the topological surface state (TSS). (d)-(f) Same as in (a)-(c) for 0.3 monolayer (ML)  $\text{Er}/\text{Bi}_2\text{Se}_2\text{Te}$ , showing the trigonal-warping of the TSS. TSS bandmaps along the  $\bar{\Gamma}\bar{M}$  direction (red and blue dashed lines in (a) and (d)) for (g) pristine and (h) 0.3 ML  $\text{Er}/\text{Bi}_2\text{Se}_2\text{Te}$ , acquired with a photon energy  $h\nu = 52$  eV and at  $T = 15$  K. Momentum distribution curves (MDCs) extracted at the  $E_F$  are shown on top of each bandmap. The induction of a trigonal warping in the TSS is also evidenced by the Fermi wavevector  $k_F$  and Fermi velocity  $v_F$  asymmetry around the  $\bar{\Gamma}$  point for the Er-doped system in (h).

To introduce the effect of the RE dopants in the former Hamiltonian (Eq. 1), a magnetic

moment can be coupled to the TI TSS via an exchange interaction<sup>42</sup> through a Zeeman-like term. The Hamiltonian takes the final form (see SM<sup>46</sup>):

$$H = \hbar v_F(k_x \sigma_y - k_y \sigma_x) + (\lambda k^3 \cos 3\theta - \Delta) \sigma_z, \quad (2)$$

where  $\Delta$  stands for the exchange coupling and  $\theta$  for the azimuthal angle of momentum.  $\Delta$  is a fitting parameter of our model. By fixing  $v_F$  and  $\lambda$ , a value of  $\Delta = 0.12$  eV is obtained by comparing the theoretical CE maps (right-hand side of Fig. 4(b)) to the experimental ones (Figs. 3(d)-(f)). Note that the  $E_F$  (with respect to the DP) is modified by the introduction of the RE dopants (Figs. 3(g)-(h)), so the values of the energies for the theoretical CE maps have been accordingly changed.

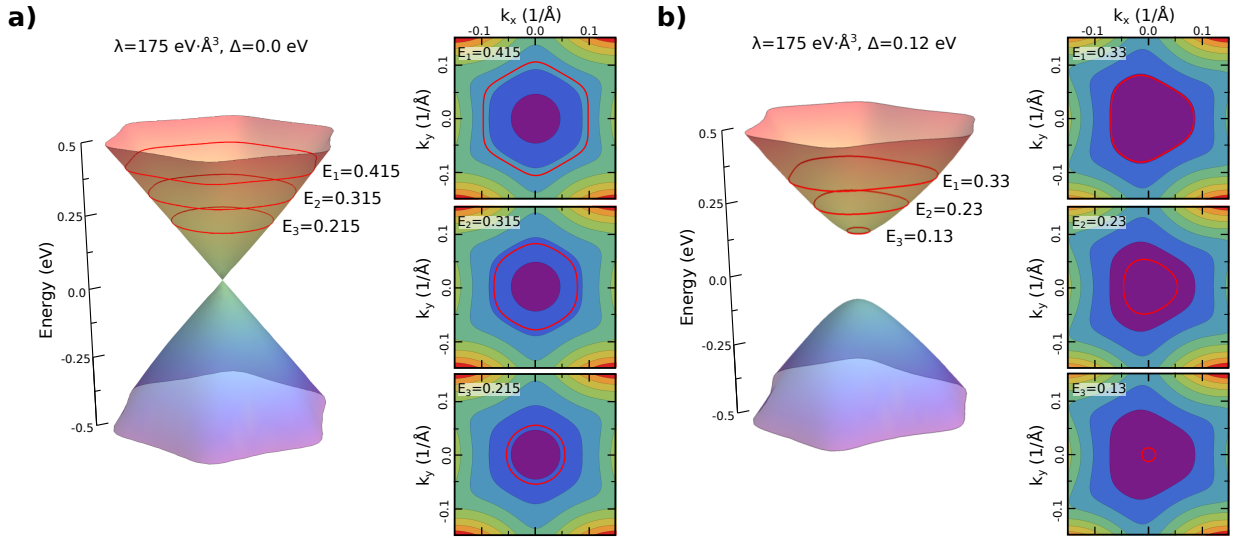


**Figure 4: Theoretical modelling of the TSS band structure and the warping transition.** Band structure of the surface state of a topological insulator and the evolution of the constant energy (CE) maps (red lines) as a function of the Fermi energy for the (a) pristine system, with  $v_F = 6.0 \cdot 10^5$  m/s and  $\lambda = 175$  eV $\cdot\text{\AA}^3$ , and (b) the system with magnetic impurities, with  $\Delta = 0.12$  eV. The transition from a six-fold to a trigonal warping, as well as the induction of a gap, is observed. The small panels display CE maps at three different energies relative to the Dirac point, corresponding to the energies of the experimental ones

The energy dispersion of the system with the above set of parameters is shown on the left-hand side of Fig. 4(b), with the TSS band presenting a gap of 240 meV as a consequence

of the non-vanishing net magnetization induced by the magnetic dopants. Furthermore, the TRS is broken and the surface of the TI becomes a quantum anomalous Hall (or Chern) insulator<sup>1,59</sup>. As seen on the CE maps (right-hand side of Fig. 4(b)), the TRS breakdown results in the transition from the six-fold to a three-fold rotational symmetry (SM<sup>46</sup>), so that the warped FS evolves from hexagonal (pristine) to trigonal (doped system), as in the experiments (Figs. 3(d)-(f)). Interestingly, the obtained value of  $\Delta$  is up to one order of magnitude larger than previous expectations<sup>60-63</sup>. Although higher values have been predicted or expected<sup>64,65</sup>, up to our knowledge, this is the first time that the exchange coupling has been estimated by direct comparison to experimental results. Such a relatively high value of the exchange coupling  $\Delta$  makes Bi<sub>2</sub>Se<sub>2</sub>Te doped with RE a good candidate system for the realization of the QAHE.

Experimentally, the change in the warping symmetry is also evidenced by the induced inversion asymmetry in the TSS band dispersion in Figs. 3(g)-(h), measured along the  $\overline{\Gamma\text{M}}$  direction (red and blue dashed lines in Figs. 3(a) and (d)), and in the momentum distribution curves (MDCs) close to the  $E_F$ , depicted above each TSS bandmap. The Fermi wavevectors  $k_F$  for 0.3 ML Er/Bi<sub>2</sub>Se<sub>2</sub>Te (blue MDC, Fig. 3(h)) are asymmetric with respect to the  $\overline{\Gamma}$  point, as compared to pristine Bi<sub>2</sub>Se<sub>2</sub>Te (red MDC, Fig. 3(g)), as a consequence of the different  $v_F$  of the two branches of the TSSs. A similar asymmetric band dispersion of the TSS was predicted for the MnBi<sub>2</sub>Te<sub>4</sub>(0001) surface AFM state alongside the same TSS warping transition<sup>43</sup>.

The evolution of the TSS as a function of the Er coverage is shown in Fig. 5. TSS ARPES bandmaps along the  $\overline{\Gamma\text{M}}$  direction for pristine, 0.15, 0.3 and 0.6 ML Er/Bi<sub>2</sub>Se<sub>2</sub>Te are shown in Figs. 5(a)-(d), respectively. The corresponding energy distribution curves (EDCs) as a function of the Er coverage are presented in Figs. 5(e)-(h), where the EDCs acquired precisely at the  $\overline{\Gamma}$  point and thus crossing the DP (along vertical dashed lines in Figs. 5(a)-(d)) are highlighted following the color correspondence. Here, orange, cyan, green, and red lines stand for pristine, 0.15, 0.3, and 0.6 ML Er/Bi<sub>2</sub>Se<sub>2</sub>Te, respectively. The band dispersions have been obtained from the EDCs fitting, whose results are indicated by red and blue dots

in Fig. 5. The dispersion obtained from the pristine sample (Figs. 5(a) and (e)) displays linear branches which clearly cross at the DP. Red and blue dots for the doped samples (Figs. 5(b)-(h)), indicate the upper and bottom band dispersions relative to the DP.

As previously described, the transition from hexagonal to trigonal of the TSS symmetry when an out-of-plane magnetic moment is introduced is expected to be accompanied by a bandgap opening at the DP because of the TRS breaking<sup>42</sup>.

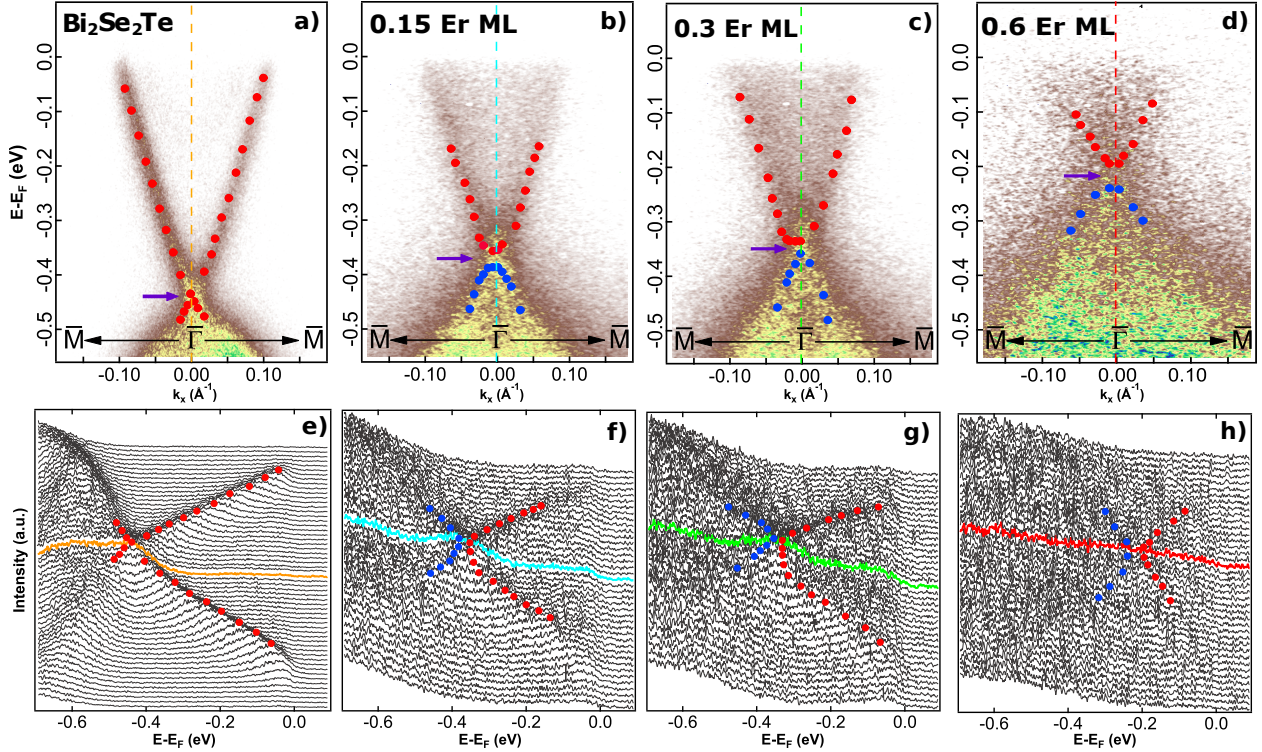


**Figure 5: Topological surface state (TSS) band structure evolution upon Er doping showing signatures of the magnetically induced bandgap at the Dirac point.** (a)-(d) TSS bandmaps for pristine  $\text{Bi}_2\text{Se}_2\text{Te}$  and 0.15, 0.3 and 0.6 Er monolayer (ML)/ $\text{Bi}_2\text{Se}_2\text{Te}$ , respectively, acquired with a photon energy of  $h\nu = 52$  eV and at  $T = 15$  K. (e)-(f) EDCs extracted from the TSS bandmaps in (a)-(d). EDCs at the  $\bar{\Gamma}$  point are highlighted following the color correspondence. TSS dispersions are obtained by fitting the EDCs and are indicated by blue and red dots for upper and bottom bands with respect to the DP, respectively. Purple arrows indicate the DP energy, which is upshifted as the Er coverage is increased.

A more detailed and comprehensive picture on the TSS band dispersion around the DP can be gathered from the EDCs fits (Figs. 5(e)-(h)); particularly, in those obtained at the  $\bar{\Gamma}$  point, extracted along vertical dashed lines in Figs. 5(a)-(d), and highlighted in the same

colors as in Fig. 5(e)-(h). For the pristine sample (Fig. 5(e)) the DP is clearly defined by the intersection of the two linear dispersive branches (orange) resulting in a single, punctual, sharp maximum of intensity at  $\sim 415$  meV. After the Er deposition, a broadening of the intensity is clearly evidenced around the DP, which would be an indication of a possible bandgap opening at the DP. This can be more clearly seen by following the band dispersion from the EDCs (red and blue dots in Figs. 5(f)-(g)). The characteristic linear dispersion of relativistic massless Dirac fermions of the pristine sample seems to be renormalized to a parabolic-like dispersion, showing a plateau in the EDC intensity in the vicinity of the  $\bar{\Gamma}$  point. This would be an indication of the bandgap between the top of the bulk valence band and the bottom of the surface state. Similar XPS and ARPES results have been found after 0.3 Dy ML deposition and are summarized in the SM<sup>46</sup>, Fig.S6.

As discussed at the beginning of the manuscript, similar bandgap openings have already been experimentally observed and attributed to TRS by magnetic impurities for numerous transition metal magnetic impurities<sup>7</sup> or Dy substitutional dopants<sup>37</sup>. Nevertheless, the magnetically induced warping transition also resulting from the TRS breaking has not been reported so far.

In this work, by doping the surface of a TI with RE atoms, the magnetically induced evolution of the warping of the TSS from hexagonal to trigonal has been demonstrated by means of ARPES experiments. This shape transition has been predicted to be accompanied by a bandgap opening at the DP and, indeed, signatures of such effect have also been observed in the present study. Additionally, the DP has been proven to be tunable towards the  $E_F$  through charge transfer between the RE adatoms and the substrate. The TSS band dispersion of the doped system is reproduced by including a Zeeman-like term in the low energy Hamiltonian describing the system. This modification entails two important consequences, being the first of them the just above-described breaking of the hexagonal symmetry and, the second one, the opening of a gap at the DP of the TSS. Both phenomena have been observed in the ARPES measurements. Moreover, we find that, in order to

theoretically describe the experimental results, a large exchange coupling is needed, of the order of 0.1 eV. Thus, the large exchange coupling and the DP tunability make the controlled doping of TIs with REs an excellent approach to realize the QAHE at higher temperatures.

## Acknowledgments

IMDEA Nanociencia and IFIMAC acknowledge financial support from the Spanish Ministry of Science and Innovation through, respectively, ‘Severo Ochoa’ (Grant CEX2020-001039-S) and ‘María de Maeztu’ (Grant CEX2018-000805-M) Programmes for Centres of Excellence in R&D. This project has received funding from the Community of Madrid (CM) through project P2018/NMT-4321 (NANOMAGCOST), from Spanish Ministry of Economic Affairs and Digital Transformation (MINECO) through projects SPGC2018-098613-B-C21 (SpOrQuMat), EQC2019-006304-P (Equipamiento científico) and PID2020-116181RB-C31 (SONANOBRAIN), and from Spanish Ministry of Science and Innovation (MICINN) and the Spanish Research Agency (AEI/10.13039/501100011033) through grants PID2021-123776NB-C21 (CONPHASE<sup>TM</sup>), PID2019-107338RB-C65 and PID2019-111773RB-I00. ICN2 was funded by the CERCA Programme/Generalitat de Catalunya and supported by the Spanish Ministry of Economy and Competitiveness, MINECO under Contract No. SEV-2017-0706. A.I.F., V.M. and S.O.V. acknowledge support from European Union’s Horizon 2020 FET-PROACTIVE project TOCHA under Grant Agreement No. 824140. LOREA was co-funded by the European Regional Development Fund (ERDF) within the Framework of the Smart Growth Operative Programme 2014-2020. B.M.C. acknowledges support from CM (PEJD-2019-PRE/IND-17048). F.G. and P.A.P. acknowledge support from the European Commission, within the Graphene Flagship, Core 3 (Grant No. 881603) and from CM (Grant NMAT2D). Y.F. acknowledges financial support through the Programa de Atracción de Talento de la Comunidad de Madrid, Spain, Grant No. 2018-T2/IND-11088. A.I.F. is a Serra Hünter fellow.

## References

- (1) Hasan, M. Z.; Kane, C. L. *Colloquium: Topological insulators. Reviews of Modern Physics* **2010**, *82*, 3045.
- (2) Moore, J. E. *The birth of topological insulators. Nature* **2010**, *464*, 194–198.
- (3) Liu, J.; Hesjedal, T. *Magnetic topological insulator heterostructures: A review. Advanced Materials* **2021**, 2102427.
- (4) Yu, R.; Zhang, W.; Zhang, H.-J.; Zhang, S.-C.; Dai, X.; Fang, Z. *Quantized anomalous Hall effect in magnetic topological insulators. Science* **2010**, *329*, 61–64.
- (5) Fei, F.; Zhang, S.; Zhang, M.; Shah, S. A.; Song, F.; Wang, X.; Wang, B. *The material efforts for quantized Hall devices based on topological insulators. Advanced Materials* **2020**, *32*, 1904593.
- (6) Xu, S.-Y.; Neupane, M.; Liu, C.; Zhang, D.; Richardella, A.; Andrew Wray, L.; Alidoust, N.; Leandersson, M.; Balasubramanian, T.; Sánchez-Barriga, J., et al. *Hedgehog spin texture and Berry's phase tuning in a magnetic topological insulator. Nature Physics* **2012**, *8*, 616–622.
- (7) Chen, Y.; Chu, J.-H.; Analytis, J.; Liu, Z.; Igarashi, K.; Kuo, H.-H.; Qi, X.; Mo, S.-K.; Moore, R.; Lu, D., et al. *Massive Dirac fermion on the surface of a magnetically doped topological insulator. Science* **2010**, *329*, 659–662.
- (8) Sessi, P.; Růkmann, P.; Bathon, T.; Barla, A.; Kokh, K.; Tereshchenko, O.; Fauth, K.; Mahatha, S.; Valbuena, M.; Godey, S., et al. *Superparamagnetism-induced mesoscopic electron focusing in topological insulators. Physical Review B* **2016**, *94*, 075137.
- (9) Růkmann, P.; Mahatha, S. K.; Sessi, P.; Valbuena, M. A.; Bathon, T.; Fauth, K.; Godey, S.; Mugarza, A.; Kokh, K. A.; Tereshchenko, O. E., et al. *Towards microscopic*

- control of the magnetic exchange coupling at the surface of a topological insulator. Journal of Physics: Materials* **2018**, *1*, 015002.
- (10) Otrokov, M. M.; Menshchikova, T. V.; Rusinov, I.; Vergniory, M.; Kuznetsov, V. M.; Chulkov, E. V. *Magnetic extension as an efficient method for realizing the quantum anomalous hall state in topological insulators. JETP Letters* **2017**, *105*, 297–302.
- (11) Kandala, A.; Richardella, A.; Rench, D.; Zhang, D.; Flanagan, T.; Samarth, N. *Growth and characterization of hybrid insulating ferromagnet-topological insulator heterostructure devices. Applied Physics Letters* **2013**, *103*, 202409.
- (12) Hou, Y.; Kim, J.; Wu, R. *Magnetizing topological surface states of  $Bi_2Se_3$  with a  $CrI_3$  monolayer. Science advances* **2019**, *5*, eaaw1874.
- (13) Chang, C.-Z.; Zhang, J.; Feng, X.; Shen, J.; Zhang, Z.; Guo, M.; Li, K.; Ou, Y.; Wei, P.; Wang, L.-L., et al. *Experimental observation of the quantum anomalous Hall effect in a magnetic topological insulator. Science* **2013**, *340*, 167–170.
- (14) Chang, C.-Z.; Zhao, W.; Kim, D. Y.; Zhang, H.; Assaf, B. A.; Heiman, D.; Zhang, S.-C.; Liu, C.; Chan, M. H.; Moodera, J. S. *High-precision realization of robust quantum anomalous Hall state in a hard ferromagnetic topological insulator. Nature Materials* **2015**, *14*, 473–477.
- (15) Otrokov, M. M.; Klimovskikh, I. I.; Bentmann, H.; Estyunin, D.; Zeugner, A.; Aliev, Z. S.; Gaß, S.; Wolter, A.; Koroleva, A.; Shikin, A. M., et al. *Prediction and observation of an antiferromagnetic topological insulator. Nature* **2019**, *576*, 416–422.
- (16) Rienks, E. D.; Wimmer, S.; Sánchez-Barriga, J.; Caha, O.; Mandal, P. S.; Růžička, J.; Ney, A.; Steiner, H.; Volobuev, V. V.; Groß, H., et al. *Large magnetic gap at the Dirac point in  $Bi_2Te_3/MnBi_2Te_4$  heterostructures. Nature* **2019**, *576*, 423–428.

- (17) Garnica, M.; Otrokov, M. M.; Aguilar, P. C.; Klimovskikh, I.; Estyunin, D.; Aliev, Z. S.; Amiraslanov, I. R.; Abdullayev, N. A.; Zverev, V. N.; Babanly, M. B., et al. *Native point defects and their implications for the Dirac point gap at MnBi<sub>2</sub>Te<sub>4</sub> (0001)*. *npj Quantum Materials* **2022**, *7*, 1–9.
- (18) Grauer, S.; Schreyeck, S.; Winnerlein, M.; Brunner, K.; Gould, C.; Molenkamp, L. *Coincidence of superparamagnetism and perfect quantization in the quantum anomalous Hall state*. *Physical Review B* **2015**, *92*, 201304.
- (19) Pan, L.; Liu, X.; He, Q. L.; Stern, A.; Yin, G.; Che, X.; Shao, Q.; Zhang, P.; Deng, P.; Yang, C.-Y., et al. *Probing the low-temperature limit of the quantum anomalous Hall effect*. *Science advances* **2020**, *6*, eaaz3595.
- (20) Gambardella, P.; Rusponi, S.; Veronese, M.; Dhési, S.; Grazioli, C.; Dallmeyer, A.; Cabria, I.; Zeller, R.; Dederichs, P.; Kern, K., et al. *Giant magnetic anisotropy of single cobalt atoms and nanoparticles*. *Science* **2003**, *300*, 1130–1133.
- (21) Wray, L. A.; Xu, S.-Y.; Xia, Y.; Hsieh, D.; Fedorov, A. V.; Hor, Y. S.; Cava, R. J.; Bansil, A.; Lin, H.; Hasan, M. Z. *A topological insulator surface under strong Coulomb, magnetic and disorder perturbations*. *Nature Physics* **2011**, *7*, 32–37.
- (22) Scholz, M.; Sánchez-Barriga, J.; Marchenko, D.; Varykhalov, A.; Volykhov, A.; Yashina, L.; Rader, O. *Tolerance of topological surface states towards magnetic moments: Fe on Bi<sub>2</sub>Se<sub>3</sub>*. *Physical Review Letters* **2012**, *108*, 256810.
- (23) Valla, T.; Pan, Z.-H.; Gardner, D.; Lee, Y.; Chu, S. *Photoemission spectroscopy of magnetic and nonmagnetic impurities on the surface of the Bi<sub>2</sub>Se<sub>3</sub> topological insulator*. *Physical Review Letters* **2012**, *108*, 117601.
- (24) Honolka, J.; Khajetoorians, A.; Sessi, V.; Wehling, T.; Stepanow, S.; Mi, J.-L.; Iversen, B.; Schlenk, T.; Wiebe, J.; Brookes, N., et al. *In-plane magnetic anisotropy of Fe atoms on Bi<sub>2</sub>Se<sub>3</sub>(111)*. *Physical Review Letters* **2012**, *108*, 256811.

- (25) Beidenkopf, H.; Roushan, P.; Seo, J.; Gorman, L.; Drozdov, I.; Hor, Y. S.; Cava, R. J.; Yazdani, A. *Spatial fluctuations of helical Dirac fermions on the surface of topological insulators. Nature Physics* **2011**, *7*, 939–943.
- (26) Chang, C.-Z.; Zhang, J.; Liu, M.; Zhang, Z.; Feng, X.; Li, K.; Wang, L.-L.; Chen, X.; Dai, X.; Fang, Z., et al. *Thin films of magnetically doped topological insulator with carrier-independent long-range ferromagnetic order. Advanced materials* **2013**, *25*, 1065–1070.
- (27) Zhang, J.; Chang, C.-Z.; Tang, P.; Zhang, Z.; Feng, X.; Li, K.; Wang, L.-L.; Chen, X.; Liu, C.; Duan, W., et al. *Topology-driven magnetic quantum phase transition in topological insulators. Science* **2013**, *339*, 1582–1586.
- (28) Vobornik, I.; Panaccione, G.; Fujii, J.; Zhu, Z.-H.; Offi, F.; Salles, B. R.; Borgatti, F.; Torelli, P.; Rueff, J. P.; Ceolin, D., et al. *Observation of distinct bulk and surface chemical environments in a topological insulator under magnetic doping. The Journal of Physical Chemistry C* **2014**, *118*, 12333–12339.
- (29) Abdalla, L. B.; Seixas, L.; Schmidt, T.; Miwa, R.; Fazzio, A. *Topological insulator  $\text{Bi}_2\text{Se}_3(111)$  surface doped with transition metals: An ab initio investigation. Physical Review B* **2013**, *88*, 045312.
- (30) Jensen, J.; Mackintosh, A. R. *Rare earth magnetism*; Clarendon Press Oxford, 1991.
- (31) Harrison, S.; Collins-McIntyre, L.; Zhang, S.; Baker, A.; Figueroa, A.; Kellock, A.; Pushp, A.; Parkin, S.; Harris, J.; Van Der Laan, G., et al. *Study of Dy-doped  $\text{Bi}_2\text{Te}_3$ : thin film growth and magnetic properties. Journal of Physics: Condensed Matter* **2015**, *27*, 245602.
- (32) Ormaza, M.; Fernández, L.; Ilyn, M.; Magana, A.; Xu, B.; Verstraete, M.; Gastaldo, M.; Valbuena, M.; Gargiani, P.; Mugarza, A., et al. *High temperature ferromagnetism in a  $\text{GdAg}_2$  monolayer. Nano Letters* **2016**, *16*, 4230–4235.

- (33) Fernández, L.; Blanco-Rey, M.; Castrillo-Bodero, R.; Ilyn, M.; Ali, K.; Turco, E.; Corso, M.; Ormaza, M.; Gargiani, P.; Valbuena, M. A., et al. *Influence of 4f filling on electronic and magnetic properties of rare earth-Au surface compounds. Nanoscale* **2020**, *12*, 22258–22267.
- (34) Fornari, C. I.; Bentmann, H.; Morelhão, S. L.; Peixoto, T. R.; Rappl, P. H.; Tcakaev, A.-V.; Zabolotnyy, V.; Kamp, M.; Lee, T.-L.; Min, C.-H., et al. *Incorporation of europium in  $Bi_2Te_3$  topological insulator epitaxial films. The Journal of Physical Chemistry C* **2020**, *124*, 16048–16057.
- (35) Tcakaev, A.; Zabolotnyy, V. B.; Fornari, C. I.; Rüßmann, P.; Peixoto, T. R.; Stier, F.; Dettbarn, M.; Kagerer, P.; Weschke, E.; Schierle, E., et al. *Incipient antiferromagnetism in the Eu-doped topological insulator  $Bi_2Te_3$ . Physical Review B* **2020**, *102*, 184401.
- (36) Kim, J.; Lee, K.; Takabatake, T.; Kim, H.; Kim, M.; Jung, M.-H. *Magnetic transition to antiferromagnetic phase in gadolinium substituted topological insulator  $Bi_2Te_3$ . Scientific Reports* **2015**, *5*, 10309.
- (37) Harrison, S.; Collins-McIntyre, L. J.; Schönherr, P.; Vailionis, A.; Srot, V.; van Aken, P. A.; Kellock, A.; Pushp, A.; Parkin, S.; Harris, J., et al. *Massive Dirac fermion observed in lanthanide-doped topological insulator thin films. Scientific reports* **2015**, *5*, 15767.
- (38) Hesjedal, T. *Rare earth doping of topological insulators: A brief review of thin film and heterostructure systems. Physica Status Solidi A* **2019**, *216*, 1800726.
- (39) Figueroa, A. I.; Bonell, F.; Cuxart, M.; Valvidares, M.; Gargiani, P.; van der Laan, G.; Mugarza, A.; Valenzuela, S. O. *Absence of Magnetic Proximity Effect at the Interface of  $Bi_2Se_3$  and  $(Bi, Sb)_2Te_3$  with EuS. Physical Review Letters* **2020**, *125*, 226801.
- (40) He, K.  *$MnBi_2Te_4$ -family intrinsic magnetic topological materials. npj Quantum Materials* **2020**, *5*, 90.

- (41) Imai, Y.; Yamaguchi, T.; Yamakage, A.; Kohno, H. *Spintronic properties of topological surface Dirac electrons with hexagonal warping*. *Physical Review B* **2021**, *103*, 054402.
- (42) Naselli, G.; Moghaddam, A. G.; Di Napoli, S.; Vildosola, V.; Fulga, I. C.; van den Brink, J.; Facio, J. I. *Magnetic warping in topological insulators*. *Physical Review Research* **2022**, *4*, 033198.
- (43) Tan, H.; Kaplan, D.; Yan, B. *Momentum-inversion symmetry breaking on the Fermi surface of magnetic topological insulators*. *Physical Review Materials* **2022**, *6*, 104204.
- (44) Wang, D.; Wang, H.; Xing, D.; Zhang, H. *Three-Dirac-fermion approach to unexpected gapless surface states of van der Waals magnetic topological insulators*. *arXiv preprint arXiv:2205.08204* **2022**,
- (45) Wang, L.-L.; Johnson, D. D. *Ternary tetradymite compounds as topological insulators*. *Physical Review B* **2011**, *83*, 241309.
- (46) See Supplemental Materials for the description of the growth process, the Er coverage calculation, further XPS and ARPES measurements and the derivation of the theoretical model. URL\_will\_be\_inserted\_by\_publisher.
- (47) García, G.; Martín, M.; Ynsa, M.; Torres-Costa, V.; Crespillo, M.; Tardío, M.; Olivares, J.; Bosia, F.; Peña-Rodríguez, O.; Nicolas, J., et al. *Process design for the manufacturing of soft X-ray gratings in single-crystal diamond by high-energy heavy-ion irradiation*. *The European Physical Journal Plus* **2022**, *137*, 1157.
- (48) Crisol, A.; Bisti, F.; Colldelram, C.; Llonch, M.; Molas, B.; Monge, R.; Nicolás, J.; Nikitina, L.; Quispe, M.; Ribó, L.; Tallarida, M. *ALBA BL20 New Monochromator Design*. Proc. MEDSI'20. 2021; pp 14–16.
- (49) Banister, J.; Legvold, S.; Spedding, F. *Structure of Gd, Dy, and Er at low temperatures*. *Physical Review* **1954**, *94*, 1140.

- (50) Maaß, H.; Schreyeck, S.; Schatz, S.; Fiedler, S.; Seibel, C.; Lutz, P.; Karczewski, G.; Bentmann, H.; Gould, C.; Brunner, K., et al. *Electronic structure and morphology of epitaxial  $\text{Bi}_2\text{Te}_2\text{Se}$  topological insulator films*. *Journal of Applied Physics* **2014**, *116*, 193708.
- (51) Walsh, L. A.; Smyth, C. M.; Barton, A. T.; Wang, Q.; Che, Z.; Yue, R.; Kim, J.; Kim, M. J.; Wallace, R. M.; Hinkle, C. L. *Interface chemistry of contact metals and ferromagnets on the topological insulator  $\text{Bi}_2\text{Se}_3$* . *The Journal of Physical Chemistry C* **2017**, *121*, 23551–23563.
- (52) Cuxart, M. G.; Valbuena, M. A.; Robles, R.; Moreno, C.; Bonell, F.; Sauthier, G.; Imaz, I.; Xu, H.; Nistor, C.; Barla, A., et al. *Molecular approach for engineering interfacial interactions in magnetic/topological insulator heterostructures*. *ACS Nano* **2020**, *14*, 6285–6294.
- (53) Miyamoto, K.; Kimura, A.; Okuda, T.; Miyahara, H.; Kuroda, K.; Namatame, H.; Taniguchi, M.; Ereemeev, S.; Menshchikova, T. V.; Chulkov, E. V., et al. *Topological surface states with persistent high spin polarization across the Dirac point in  $\text{Bi}_2\text{Te}_2\text{Se}$  and  $\text{Bi}_2\text{Se}_2\text{Te}$* . *Physical Review Letters* **2012**, *109*, 166802.
- (54) Bao, L.; He, L.; Meyer, N.; Kou, X.; Zhang, P.; Chen, Z.-g.; Fedorov, A. V.; Zou, J.; Riedemann, T. M.; Lograsso, T. A., et al. *Weak anti-localization and quantum oscillations of surface states in topological insulator  $\text{Bi}_2\text{Se}_2\text{Te}$* . *Scientific Reports* **2012**, *2*, 726.
- (55) Fu, L. *Hexagonal warping effects in the surface states of the topological insulator  $\text{Bi}_2\text{Te}_3$* . *Physical Review Letters* **2009**, *103*, 266801.
- (56) Chen, Y.; Analytis, J. G.; Chu, J.-H.; Liu, Z.; Mo, S.-K.; Qi, X.-L.; Zhang, H.; Lu, D.; Dai, X.; Fang, Z., et al. *Experimental realization of a three-dimensional topological insulator,  $\text{Bi}_2\text{Te}_3$* . *Science* **2009**, *325*, 178–181.

- (57) Arakane, T.; Sato, T.; Souma, S.; Kosaka, K.; Nakayama, K.; Komatsu, M.; Takahashi, T.; Ren, Z.; Segawa, K.; Ando, Y. *Tunable Dirac cone in the topological insulator  $Bi_{2-x}Sb_xTe_{3-y}Se_y$* . *Nature Communications* **2012**, *3*, 636.
- (58) Xia, Y.; Qian, D.; Hsieh, D.; Wray, L.; Pal, A.; Lin, H.; Bansil, A.; Grauer, D.; Hor, Y. S.; Cava, R. J., et al. *Observation of a large-gap topological-insulator class with a single Dirac cone on the surface*. *Nature Physics* **2009**, *5*, 398–402.
- (59) Qi, X.-L.; Wu, Y.-S.; Zhang, S.-C. *Topological quantization of the spin Hall effect in two-dimensional paramagnetic semiconductors*. *Physical Review B* **2006**, *74*, 085308.
- (60) Nomura, K.; Nagaosa, N. *Electric charging of magnetic textures on the surface of a topological insulator*. *Physical Review B* **2010**, *82*, 161401.
- (61) Yokoyama, T.; Zang, J.; Nagaosa, N. *Theoretical study of the dynamics of magnetization on the topological surface*. *Physical Review B* **2010**, *81*, 241410.
- (62) Yokoyama, T. *Current-induced magnetization reversal on the surface of a topological insulator*. *Phys. Rev. B* **2011**, *84*, 113407.
- (63) Ferreiros, Y.; Buijnsters, F.; Katsnelson, M. *Dirac electrons and domain walls: A realization in junctions of ferromagnets and topological insulators*. *Physical Review B* **2015**, *92*, 085416.
- (64) Liu, Q.; Liu, C.-X.; Xu, C.; Qi, X.-L.; Zhang, S.-C. *Magnetic impurities on the surface of a topological insulator*. *Physical Review Letters* **2009**, *102*, 156603.
- (65) Ferreiros, Y.; Cortijo, A. *Domain wall motion in junctions of thin-film magnets and topological insulators*. *Physical Review B* **2014**, *89*, 024413.